Trajectory Surface Hopping Study of the O(^{3}P) + Ethylene Reaction Dynamics†

Wenfang Hu,‡ György Lendvay,§ Biswajit Maiti,# and George C. Schatz*,‡

Department of Chemistry, Northwestern University, Evanston Illinois 60208-3113, Chemical Research Center, Hungarian Academy of Sciences, H-1525 Budapest, P.O. Box 17, Hungary, and Department of Chemistry, Faculty of Science, Banaras Hindu University, Varanasi 221005, India

Received: August 21, 2007; In Final Form: October 14, 2007

Spin−orbit coupling (SOC) induced intersystem crossing (ISC) has long been believed to play a crucial role in determining the product distributions in the O(^{3}P) + C_2H_4 reaction. In this paper, we present the first nonadiabatic dynamics study of the title reaction at two center-of-mass collision energies: 0.56 eV, which is barely above the H-atom abstraction barrier on the triplet surface, and 3.0 eV, which is in the hyperthermal regime. The calculations were performed using a quasiclassical trajectory surface hopping (TSH) method with the potential energy surface generated on the fly at the unrestricted B3LYP/6-31G(d,p) level of theory. To simplify our calculations, nonadiabatic transitions were only considered when the singlet surface intersects the triplet surface. At the crossing points, Landau−Zener transition probabilities were computed assuming a fixed spin−orbit coupling parameter, which was taken to be 70 cm^{-1} in most calculations. Comparison with a recent crossed molecular beam experiment at 0.56 eV collision energy shows qualitative agreement as to the primary product branching ratios, with the CH_3 + CHO and H + CH_2CHO channels accounting for over 70% of total product formation. However, our direct dynamics TSH calculations overestimate ISC so that the total triplet/singlet ratio is 25:75, compared to the observed 43:57. Smaller values of SOC reduce ISC, resulting in better agreement with the experimental product relative yields; we demonstrate that these smaller SOC values are close to being consistent with estimates based on CASSCF calculations. As the collision energy increases, ISC becomes much less important and at 3.0 eV, the triplet to singlet branching ratio is 71:29. As a result, the triplet products CH_2 + CH_2O, H + CH_2CHO and OH + C_2H_3 dominate over the singlet products CH_3 + CHO, H_2 + CH_2CO, etc.

1. Introduction

The reaction of triplet oxygen with ethylene has attracted much experimental and theoretical attention because it is one of the basic oxidative reactions in the combustion of many different hydrocarbon fuels.[1] This simplest O(^{3}P) + alkene reaction, however, demonstrates rather complex reaction mechanisms. The following reactions are the possible primary product channels:

$$O(^3P) + CH_2{=}CH_2 \rightarrow {}^2OH + {}^2CH_2CH \quad (R1)$$

$$O(^3P) + CH_2{=}CH_2 \rightarrow {}^{\bullet}CH_2CH_2O^{\bullet}$$

$$\rightarrow {}^2H + {}^2CH_2CHO \quad (R2)$$

$$\rightarrow {}^3CH_2 + CH_2O \quad (R3)$$

$$\rightarrow {}^2CH_3 + {}^2CHO \quad (R4)$$

$$\rightarrow {}^2H + {}^2CH_3CO \quad (R5)$$

$$\rightarrow H_2 + CH_2CO \quad (R6)$$

$$\rightarrow CO + CH_4 \quad (R7)$$

Past work has proposed[2−4] that the electrophilic oxygen atom attacks the C=C bond and forms an energetic triplet biradical $^{\bullet}CH_2CH_2O^{\bullet}$. The triplet biradical then undergoes fragmentation and rearrangement, which competes with intersystem crossing (ISC) to give the corresponding singlet biradical. Product branching in the thermal O + ethylene reaction has been a much disputed topic in the experimental chemical dynamics community,[5] but the general agreement is that the hydrogen−vinoxy (H + CH_2CHO) and the methyl−formyl (CH_3 + CHO) channels account for up to 90% of the products. Although the first of these products can be produced via dissociation of the triplet biradical, the second is usually thought of as being the result of ISC followed by 1,2-hydrogen migration to give a singlet acetaldehyde (CH_3CHO) intermediate that subsequently dissociates. The observation that the rate of the two major channels is similar suggests that dissociation of the biradical and ISC are of comparable importance. Note that there is no evidence for the occurrence of reaction channel R7 in any of the experimental measurements, even though this is the most exothermic pathway.

Theoretical studies of the reaction O(^{3}P) + C_2H_4 have largely been confined to quantum chemical calculations of the stationary points and energetics along the reaction pathways. Earlier work was concentrated on the characterization of the initial oxygen atom addition step.[6−8] It was shown that the reaction path corresponds to an asymmetric approach of O toward one of the carbon atoms of the olefin double bond. Nondynamical correlation effects had to be included to properly describe the electronic structure of the system, and a barrier height of 4.7 kcal/mol was found at the multireference configuration interaction (MRD-CI) level,[8] higher than the experimental activation energy of about 2 kcal/mol.[9] Several groups calculated various triplet and singlet states of the CH_2CH_2O biradical[7,10,11] using

† Part of the "William A. Lester, Jr., Festschrift".

* Corresponding author. E-mail: schatz@chem.northwestern.edu.
‡ Northwestern University.
§ Hungarian Academy of Sciences.
# Banaras Hindu University.

10.1021/jp076716z CCC: $40.75 © 2008 American Chemical Society
Published on Web 12/19/2007

either spin-restricted or spin-unrestricted Hartree−Fock formalism. The relative stability of the different biradical states varies in these calculations, but the small energy splitting of the triplet and singlet states supports the assumption that ISC is an important mechanism behind the title reaction.

There have been a number of theoretical efforts aimed at elucidating the reaction mechanisms on the triplet surface.[11−13] According to the generally accepted picture the $O(^3P) + C_2H_4 \rightarrow {}^3CH_2CH_2O \rightarrow H + CH_2CHO/CH_2 + CH_2O$ reactions (R2 and R3) are the energetically most accessible, with the direct H abstraction (R1) and the adduct $^3CH_2CH_2O$ isomerization pathways involving higher activation barriers. Reactions on the singlet surface involve facile rearrangement of the singlet biradical $^1CH_2CH_2O$ to several low-lying intermediate complexes including acetaldehyde, oxirane (c-C_2H_4O, ethylene oxide) and vinyl alcohol (CH_2CHOH), followed by interchange among these isomers and decomposition reactions to give $CH_3 + CHO$, $H_2 + CH_2CO$, $CH_4 + CO$, etc.[11,14,15] Although $CH_3 + CHO$ products can come from both singlet and triplet pathways, the ISC pathway has generally been assumed to be dominant.

A more comprehensive investigation of both the triplet and singlet potential surfaces was recently carried out by Nguyen et al.[16] at relatively high levels of theory including G3, CBS-QB3, G2M, and MR-CI. Using a ratio of 45:55 for total triplet to total singlet product formation rate that was inferred from the experimental kinetics and crossed beam data, they computed product distributions and thermal rate constants for the title reaction and achieved overall good agreement with the experimental product branching ratios.

Wherever possible, a dynamics description is desirable for providing a quantitative determination of the reaction mechanism, the product branching, and for visualization of chemical processes, in particular, when multiple electronic states are involved. However, dynamical simulations of nonadiabatic processes face severe obstacles, including the determination of multiple surfaces and their couplings, and describing the nuclear motion subject to these surfaces. For a multidimensional system with many degrees of freedom like O + ethylene, the traditional strategy of first generating analytical potential energy surfaces (PES) and coupling surfaces[17−19] is very difficult and has not, so far, been done. As an alternative to this, in the present study we have used direct dynamics quasiclassical trajectory calculations with trajectory surface hopping (TSH) to describe ISC. We used a simplified version of the TSH method wherein only gradients for the currently occupied surface are computed as the trajectory evolves, and hops are only allowed when crossings between the singlet and triplet surfaces are encountered. Both singlet and triplet energies are determined using the unrestricted B3LYP/6-31G(d,p) electronic structure method. Whenever a triplet−singlet (T−S) surface crossing is detected during the trajectory propagation, a decision to hop is made on the basis of the Landau−Zener transition probability formula. Comparison with the recent crossed molecular beam experiment of Casavecchia et al.[5] shows reasonable agreement as to the product distributions. Our calculations also provide a prediction of the dynamical behavior at hyperthermal energies well above the reaction barriers.

The present TSH method is most similar to one described long ago by Stine and Muckerman.[20] Neglect of hops away from crossings is physically justified because of the smallness of the spin−orbit coupling matrix elements (typically <100 cm^{-1}) compared to the singlet/triplet energy differences (typically >1000 cm^{-1}). In contrast to some of the more recent methods, such as the Tully's fewest switches method,[21] where the electronic Schrödinger equation is integrated on the fly while the trajectory evolves, the present method avoids the extra machinery and smaller time steps to do this, a simplification that is absolutely necessary to make the calculations feasible given the computational effort associated with the direct dynamics calculations. Other methods, such as the Ehrenfest method,[22−28] provide another alternative for describing nonadiabatic dynamics in which the dynamics is evolved on an effective average electronic state. This would not be useful here as there are many possible products, and the time scales for reaction vary from <1 ps to >1 μs.

Most of our calculations have considered an initial kinetic energy of 0.56 eV so as to match the conditions used in the Casavecchia experiments. We have also examined the $O(^3P) + C_2H_4$ reaction dynamics at a hyperthermal collision energy of 3.0 eV. Collisions in the hyperthermal regime are of interest for understanding material erosion of space vehicles traveling in low-Earth orbit (LEO), where the ambient oxygen atoms, and other reactive species, can collide with the vehicle surface at relative translational energies on the order of several electronvolts. Often the vehicle surfaces include polymeric components (as in thermal blankets) so the present work provides a model system for studying the importance of both singlet and triplet reaction mechanisms in degrading unsaturated hydrocarbon polymers. In addition, $O + C_2H_4$ is relevant to reactions of atomic oxygen with outgassed unsaturated hydrocarbons in LEO.

2. Computational Details

2A. Electronic Structure Calculations. The direct dynamics calculations were made by interfacing the Q-Chem computer program[29] with a molecular dynamics code so that at each point of the trajectory, the potential energy and/or gradients of the triplet and singlet ground electronic states were evaluated using the B3LYP[30,31] density functional theory (DFT) method with the 6-31G(d, p) basis set. For calculations on both surfaces, we used spin unrestricted wave functions.

To assess the quality of the UB3LYP/6-31G(d,p) surfaces, we carried out geometry optimizations for the stationary points along major reaction pathways. Harmonic vibration frequencies and zero-point vibration energies (ZPE) were computed at the same theory level. The optimized structures are characterized as transition states if only one imaginary frequency exists, or as minima if all nonzero frequencies are real. Intrinsic reaction coordinate (IRC) calculations were performed to make sure the transition states (TS) connect the expected minima on the potential surfaces. For a proper description of the biradical nature of $^{\bullet}CH_2CH_2O^{\bullet}$ in the singlet state, where the unpaired α and β electrons are separated on the terminal carbon and oxygen atoms, a multiconfiguration wave function, such as the CASSCF method, should be used. However, by forcing an unrestricted SCF procedure on the open-shell singlet biradical and the transition states that connect to it, we obtain reasonable results with single configuration calculations. To enforce spin polarization, we added 20% of the α LUMO to the α HOMO to break the $\alpha-\beta$ symmetry in the initial guess of MOs.

The magnitude of the spin−orbit coupling (SOC) is small compared to the energy difference between the surfaces for most geometries. Thus the only significant T−S transitions occur when the surfaces are very close to a crossing. To simplify our dynamical simulations, surface hops are allowed only at points where the triplet and singlet surfaces cross. Furthermore, we did not actually calculate the spin−orbit matrix elements at each

crossing point of each trajectory; instead, we used a constant value for the SOC throughout our calculations. This approximation is crude but justified if the large majority of T−S crossings occur in the vicinity of the CH_2CH_2O biradical (as is the case at low energies) where the SOC matrix elements do not vary much with geometry.[32] To verify this, we calculated the spin−orbit matrix elements at selected crossing point geometries detected in sample trajectories using the Breit−Pauli method as implemented by Fedorov and Gordon[33] in GAMESS.[34] The orbitals were generated from a twelve-state state-averaged CASSCF calculation using an aug-cc-pVDZ one electron basis set.[35] Eight electrons in eight active orbitals were included in the CASSCF. We found that the states that are close in energy and thus are actively involved in ISC processes are the first 6 triplet states 1^3A ($M_s = 0, \pm1$), 2^3A ($M_s = 0, \pm1$), and the first 2 singlet states 1^1A ($M_s = 0$), 2^1A ($M_s = 0$). The spin−orbit matrix elements between the singlet and the triplet states are complex numbers. Following a procedure proposed by Hoffmann and Schatz,[17] we combine the three components of a triplet to form symmetry-adapted triplet wavefunctions, i.e.,

$$^3\Psi_z = \mathrm{i}\,^3\Psi(M_s{=}0) \tag{1}$$

$$^3\Psi_x = \frac{1}{\sqrt{2}}[^3\Psi(M_s{=}1) + {}^3\Psi(M_s{=}-1)] \tag{2}$$

$$^3\Psi_y = \frac{i}{\sqrt{2}}[^3\Psi(M_s{=}1) - {}^3\Psi(M_s{=}-1)] \tag{3}$$

In this new representation, the matrix elements $\langle {}^1\Psi|H_{SO}|{}^3\Psi\rangle$ are all real, ranging from 0 to 70 cm^{-1}. Through close inspection of the SOC matrix, we found that the triplet wavefunctions can further be linearly combined so that the first singlet state 1^1A only strongly couples to three of the six triplet states, and the second singlet 2^1A couples to the other three triplets. From this observation, we decided to calculate an average SOC between the singlet and triplet states by summing up the squares of the 12 singlet−triplet coupling elements and dividing the sum by 6 (where 6 is the number of nonzero matrix elements after the decoupling):

$$V_{13} = \sqrt{\left[\sum_{i=1}^{2}\sum_{j=x,y,z} |\langle 1^1\Psi|H_{SO}|\mathrm{i}\,^3\Psi_j\rangle|^2 + \sum_{i=1}^{2}\sum_{j=x,y,z} |\langle 2^1\Psi|H_{SO}|\mathrm{i}\,^3\Psi_j\rangle|^2\right]/6} \tag{4}$$

Calculations at six different crossing point geometries give an average SOC of around 35 cm^{-1}. Rather than use this value, we decided to generate results for several different choices of the SOC. In the first set of results to be presented, we used a high value of 70 cm^{-1}, and not surprisingly this leads to excess singlet formation. In later results we considered 50 and 30 cm^{-1} for the SOC to assess sensitivity of the results to the value of the coupling parameter, and to determine if errors in the TSH method lead to deviations between the SOC that produces the best match with experiment and the SOC that is obtained from the CASSCF calculations.

2B. Direct Dynamics Calculations. To study ISC effects in the O(^{3}P) + C_2H_4 reaction, we have used the direct dynamics quasiclassical variant of the TSH method where the potential is calculated on the fly with density functional theory. The trajectories are initiated on the ground triplet electronic state at a reagent collision energy of 0.56 eV, to match the conditions of the crossed molecular beam (CMB) study of Casavecchia and co-workers,[5] or of 3 eV, to simulate LEO collisions. Initially, the classical mechanical equations of motion use energy and gradients from the triplet surface, but the singlet surface energy is also calculated and the singlet−triplet gap is evaluated to identify crossings. When the singlet surface intersects the triplet surface, we compute a transition probability using the Landau−Zener (LZ) formula:

$$P_{LZ} = 1 - \exp\left[-\frac{2\pi {V_{13}}^2}{\hbar\dot{Z}\left|\frac{dE_1}{dR} - \frac{dE_3}{dR}\right|}\right] \tag{5}$$

where V_{13} is the SOC between the two surfaces, $\dot{Z}$ is the nuclear coordinate velocity perpendicular to the crossing seam, and

$$\left|\frac{dE_1}{dR} - \frac{dE_3}{dR}\right|$$

is the magnitude of the difference between the singlet and triplet energy slopes at the crossing point. These slopes are determined by interpolating the gradients of the singlet and triplet surfaces, respectively, to the crossing location, using values obtained from time steps just before and just after the crossing. Thus it is only at crossing points that gradient information is required on both surfaces. We could have used the Zhu−Nakamura (ZN) expression[36,37] instead of eq 5; however, for the present application, the available energy is well above the crossing seam so the LZ and ZN probabilities are essentially the same.

Once the LZ probability is calculated, it is then compared with a random number ζ between 0 and 1 to decide if a surface hop should occur. If $P_{LZ} > \zeta$, the electronic state is switched from triplet to singlet and the trajectory is continued on the singlet surface. No momentum adjustment has to be made on the new surface because hopping only occurs at the point of intersection where $E_1 = E_3$. If $P_{LZ} < \zeta$, the trajectory continues on the triplet surface. The treatment of a switch from the singlet to the triplet state follows exactly the steps described above. No attempt is made to restrict the frequency of successive hops.

One additional aspect in our treatment of nonadiabatic transitions concerns hops in the product asymptotic region. For the products H (^{2}S) + $CH_2CHO(^2A'')$, H (^{2}S) + $CH_3CO(^2A')$, and $CH_3(^2A_2'')$ + $CHO(^2A')$, the triplet and singlet surfaces are co-incident with each other asymptotically. Hops in these regions occur but are of no consequence because the two surfaces are identical. To remove this unnecessary hopping, we set P_{LZ} equal to zero at crossing points where the products are well separated. More precisely, for a C−H separation of about 3.5 a_0 or a C−C separation of about 4.8 a_0 the two surfaces are nearly degenerate for these dissociation channels, so we cut off asymptotic hopping beyond these values.

Other features of the direct dynamics algorithm using TSH follow our previous work.[38,39] The polyatomic reactant C_2H_4 is prepared in its ground electronic and rovibrational state by running an intramolecular trajectory starting from the equilibrium geometry of C_2H_4 with kinetic energy of each normal mode made equal to the corresponding zero-point energy. This trajectory is integrated for many vibrational periods. The phase of the vibration motion is then sampled from this trajectory, and the attacking oxygen atom is randomly placed around the vibrating C_2H_4 molecule with an initial center-of-mass distance of 14 a_0, a maximum sampled impact parameter of 10 a_0, and a reagent relative translational energy of 0.56 eV. A standard fifth-order predictor, sixth-order corrector integration algorithm

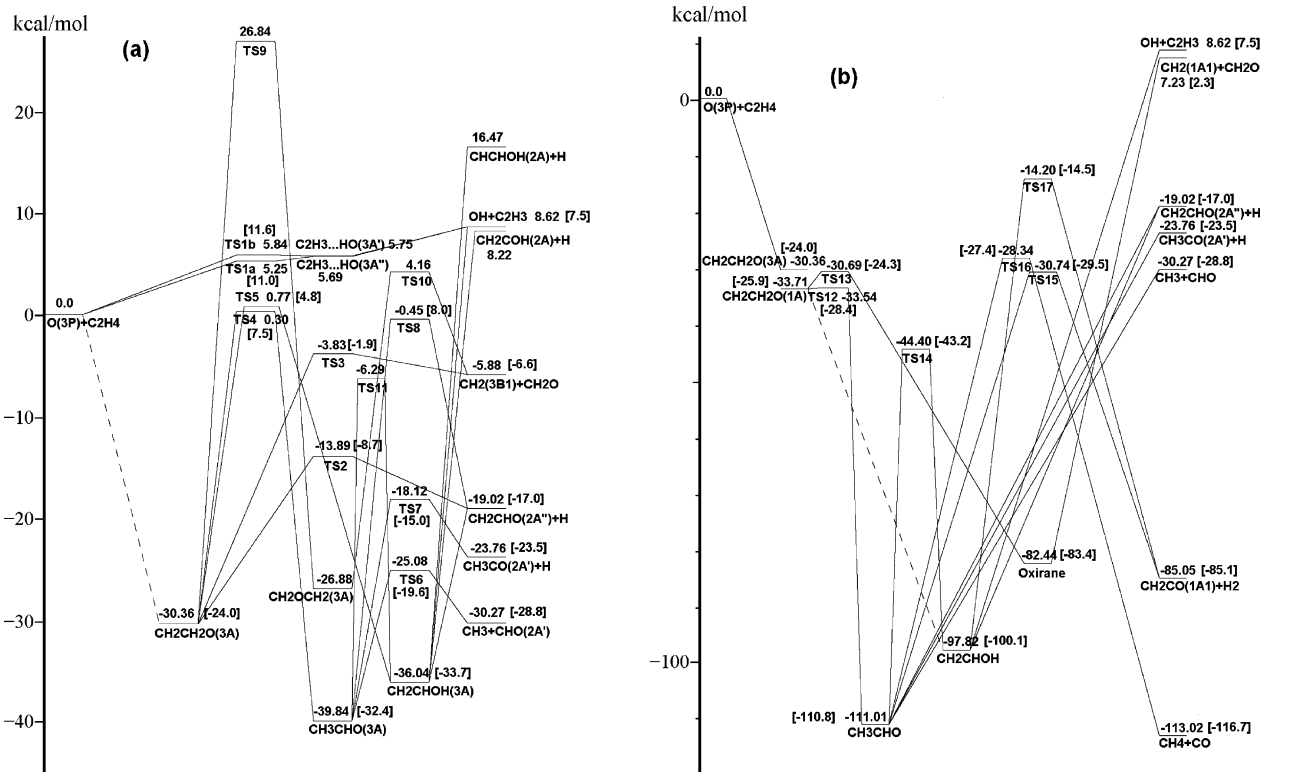

Figure 1. Potential energy profiles on (a) the triplet surface and (b) the singlet surface calculated using UB3LYP/6-31G(d,p). The values in brackets are higher quality theory calculations (the average of the values computed at the G3, CBS-QB3, and G2M levels) taken from Figures 1 and 3 in ref 16.

is employed to propagate Hamilton's equations of motion along the trajectory with an integration time step of 10 au (0.24 fs). The trajectory is terminated if the product pair is sufficiently separated (15−17 a_0) or a maximum integration step is reached. Upon completion of the trajectory propagation, a final analysis is performed to derive various dynamical properties of the products. Specifically, the reactive cross section for channel i is computed as

$$\sigma_i = \frac{2\pi b_{\max}^2}{N}\sum_{k=1}^{N} x_k P_{ik} \qquad (6)$$

in which $x_k = b_k/b_{\max}$ with b_k being the impact parameter of trajectory k and $b_{\max}$ being the maximum sampled impact parameter, N is the total number of trajectories, and P_{ik} is the characteristic function for trajectory k. P_{ik} is 1 if the trajectory yields channel i and 0 otherwise.

3. Results and Discussions

3A. Potential Energy Surfaces. Shown in Figure 1 are the computed triplet and singlet energies for the important stationary points, relative to the energy of $O(^3P) + C_2H_4$, inclusive of zero-point energies. The B3LYP/6-31G(d,p) values are compared with the values reported by Nguyen et al.,[16] for which they averaged the results of their G2M, CBS-QB3, and G3 calculations. Although the energies of the dissociation products and of the low-lying intermediates on the singlet surface agree well between the two calculations, the B3LYP values at the other stationary points are generally lower by up to 8 kcal/mol than the higher level results. This discrepancy is especially prominent for the saddle points and reaction intermediates on the triplet surface. For example, for the CH_2CH_2O biradical, the triplet and singlet state relative energies are −30.4 and −33.7 kcal/mol, respectively on the B3LYP surface, but −24.0 and −25.9 kcal/mol, respectively, according to the CASSCF(8,8) + MR-CISD+Q method.[16] However, the relative significance of the primary reaction pathways is largely preserved on the B3LYP surfaces so that isomerization of triplet CH_2CH_2O is still unfavorable compared to decomposition.

The direct H abstraction by $O(^3P)$ to form OH and C_2H_3 is the only primary channel that proceeds without going through the O addition intermediate. As noted by Nguyen and co-workers, there are two similar transition states (TS1a is of $^3A''$ symmetry, and TS1b is of $^3A'$ symmetry) involved in H abstraction. Their relative energies, however, are only 5−6 kcal/mol in our B3LYP/6-31G(d,p) calculations, even lower than that of the product OH + C_2H_3 (8.6 kcal/mol). This suggests the existence of a post-TS weakly bonded complex formed between C_2H_3 and OH radicals on the B3LYP surface. Indeed TS1a and TS1b correlate with two hydrogen-bonded $CH_2{=}CH\cdot\cdot\cdot HO$ complexes of $^3A''$ and $^3A'$ symmetry, respectively. Though the ZPE-inclusive energy of the complex $C_2H_3\cdot\cdot\cdot HO(^3A'')$ is somewhat higher than TS1a, the classical energy curve (before including the ZPE) does show a drop from TS1a to the hydrogen-bonded complex. In any event, the formation of OH + C_2H_3 is not important in the crossed-beam experiments of Casavecchia et al., so this defect in the potential surface is of minor significance to our reaction dynamics studies.

The large majority of reactions occur through the formation of the CH_2CH_2O biradical. We were unable to locate a saddle point to O addition on the B3LYP surface, and it is very likely that there is no barrier on the B3LYP PES. The recommended thermal rate coefficient has an activation energy of only 2 kcal/mol,[9] so the error caused by the lack of a barrier is again a minor issue to this work. The CH_2CH_2O biradical may exist in either the triplet or the singlet state. Our unrestricted B3LYP calculations locate the singlet biradical ∼3.3 kcal/mol below

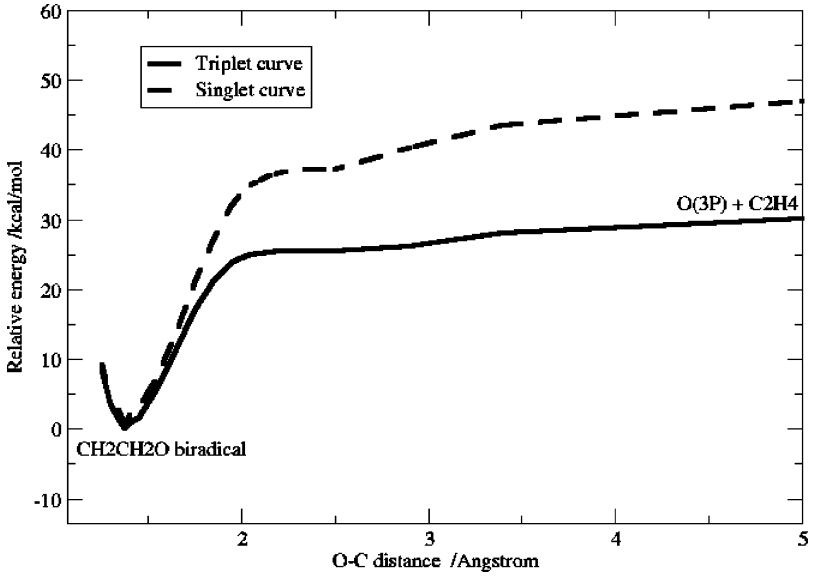

Figure 2. Crossing seam of the triplet and singlet potential energy surfaces as O(^{3}P) attacks one of the carbon atoms in ethylene to form the triplet adduct CH_2CH_2O. The triplet curve corresponds to constrained optimization at fixed C−O distances on the triplet surface. The singlet energies are calculated at the triplet optimized geometries.

the triplet state. Thus the S−T crossing can occur during the formation of the CH_2CH_2O biradical, or at any time thereafter until it dissociates. Figure 2 depicts the minimum energy path as the triplet oxygen approaches one of the carbon atoms, along with the singlet energies calculated at the optimized triplet geometries. In contrast to the analogous curves that have been constructed using multireference perturbation theory (CASPT2, Figure 2 of ref 16), the energy barrier to O addition is barely seen on the B3LYP surface. However, what is common is that the triplet and singlet curves are very close over a wide range of C−O distances (1.3−1.7 Å) in the biradical region. This means that there are numerous singlet−triplet surface crossings after the biradical complex is formed, so even though the crossing probability for each hop is typically quite small, the overall ISC probability for a long-lived intermediate can be quite large.

After the initial formation of the triplet CH_2CH_2O complex, it may subsequently isomerize to $CH_3CHO(^3A)$, CH_2CHOH (^3A), and CH_2OCH_2 (^3A) through relatively high barriers, followed by further decomposition. The energetically more accessible pathways for CH_2CH_2O are dissociation via TS2 and TS3 to produce H + $CH_2CHO(^2A'')$ and CH_2O + $CH_2(^3B_1)$, respectively. Note that barriers TS4 and TS5 corresponding to 1,2 H atom transfer to the C and O atoms, respectively, are not as high as predicted at the G2M, CBS-QB3, and G3 levels. However, they are close to the energy of the reactants on the B3LYP surface and thus are not particularly accessible under conditions that mimic the Casavecchia et al. experiment.

Reactions on the singlet surface start from $CH_2CH_2O(^1A)$. By surmounting very small barriers, CH_2CH_2O rearranges to form three low-lying intermediate complexes, $CH_3CHO(^1A')$, CH_2CHOH ($^1A'$), and the three-member ring isomer, oxirane ($^1A_1$). B3LYP failed to locate the TS leading to vinyl alcohol. There is also the possibility of direct H_2 elimination from ^{1}-CH_2CH_2O to yield H_2 and ketene. This process was observed as a minor pathway in our dynamics calculations, but the corresponding saddle point on the PES has never been found.

Acetaldehyde is the lowest-lying singlet isomer. Several dissociation channels are open to this molecule for energies accessible starting from O + C_2H_4. These include direct bond cleavage to give CH_3 + CHO, CH_3CO + H, and CH_2CHO + H, as well as concerted reactions to produce CH_4 + CO and H_2 + $CH_2CO(^1A_1)$. Vinyl alcohol is the next lowest-energy isomer and is accessible from acetaldehyde via a barrier (TS14) that is lower than any of the dissociation pathways of the latter. Fragmentation of vinyl alcohol, i.e., the C−OH and the O−H bond breakage or through TS17 to give H_2 + CH_2CO, requires much more energy. The ring-opening behavior of oxirane has been studied previously.[8] It was found that the C−O bond rupture back to singlet CH_2CH_2O is energetically favored over C−C breakage to form the biradical $^{\bullet}CH_2-O-CH_2^{\bullet}$. We were unable to characterize the C−C bond breaking reaction path with the unrestricted B3LYP calculations, including the formation of singlet CH_2OCH_2 in different face-to-face, edge-to-edge configurations as described in ref 8. The study of Wortmann-Saleh et al. indicates the possibility of S−T ISC during the oxirane ring opening via C−C bond rupture, but this is not likely to play an important role in the present simulations because isomerization of oxirane to give acetaldehyde dominates in the oxirane dynamics.

3B. Dynamics at Low Energy. In this section we present the results of our direct dynamics TSH calculations at E_{coll} = 0.56 eV (12.9 kcal/mol). This is the energy for which Casavecchia and co-workers[5] have determined the relative yields $\sigma_i/\Sigma_i\sigma_i$ (σ_i being the reactive cross section for channel i) for five primary product channels: H + CH_2CHO, CH_3 + CHO, CH_2 + H_2CO, H + CH_3CO, and H_2 + CH_2CO. Note that this collision energy is just above the H abstraction barrier (11−12 kcal/mol) reported by Nguyen et al.,[16] but 7−8 kcal/mol higher than the B3LYP/6-31G(d,p) barrier (5−6 kcal/mol). Because OH + C_2H_3 is the only endothermic reaction that involves reaction over a barrier higher than is involved in O addition, almost all previous experimental and theoretical studies disregarded this channel. Due to the low H abstraction barrier on the B3LYP surface, we expect an overestimation of this channel in our dynamical results.

For the O(^{3}P) + C_2H_4 simulations at 0.56 eV, 545 trajectories were generated, among which 143 trajectories are reactive. We initially propagated the trajectories for a maximum of 4000 steps (about 960 fs); at the end of that period the ratio of trajectories in the triplet to singlet state is 41:59. Among the reactive trajectories, 14 involve direct H abstraction by O to produce

$OH + C_2H_3$. The rest involve O addition to form the CH_2CH_2O triplet adduct. If ISC is not allowed to occur, the excess energy (collision energy + exothermicity) of the activated triplet biradical is rapidly randomized over its internal vibration modes and it can dissociate to various triplet products. However, because the system repeatedly traverses the S−T crossing seam in the vicinity of the biradical intermediate, ISC to the singlet surface is rather efficient. Out of the 129 trajectories that go through the triplet CH_2CH_2O, 81 hop to the singlet within the first 4000 steps.

The 48 reactive trajectories that remain on the triplet surface mostly decompose via C−H or C−C bond breaking to give H + CH_2CHO or $CH_2 + CH_2O$. Isomerization of the CH_2CH_2O intermediate to triplet CH_3CHO is negligible at low collision energies. Within 4000 integration steps (0.96 ps), 21 out of the 48 trajectories dissociate to give H + CH_2CHO (18 trajectories) and $CH_2 + CH_2O$ (3 trajectories). For the 27 trajectories not decayed at 4000 steps, ISC competes with decomposition in determining product yields.

After the system undergoes T−S transition, the singlet CH_2CH_2O rearranges to give oxirane (37 out of 81 trajectories), acetaldehyde (38 out of 81), and vinyl alcohol (2 out of 81) within the first 0.96 ps (most within the first 0.1 ps), along the almost barrierless isomerization reaction paths. We note that the vinyl alcohol channel is much less probable than the acetaldehyde and oxirane channels. Acetaldehyde is about 13 kcal/mol below vinyl alcohol on the PES and is thus thermodynamically more favorable. At the same time, however, oxirane lies about 15 kcal/mol above vinyl alcohol. So the prevalence of the oxirane channel over the vinyl alcohol channel can only be explained from dynamical considerations: the CH_2CH_2O ring-closure process does not have to break any molecular bond, whereas isomerization to CH_2CHOH involves concerted C−H bond breaking and O−H bond formation. Other than the aforementioned isomerization reactions, the singlet CH_2CH_2O can also decompose via direct H_2 elimination, leading to H_2 + ketene (1 out of 81 trajectories), or H elimination to produce H + CH_2CHO on the singlet surface.

The hot acetaldehyde, oxirane and vinyl alcohol formed upon CH_2CH_2O isomerization on the singlet surface can isomerize among themselves and can undergo further decomposition to various products. For oxirane, the dissociation channels are energetically much more demanding than the ring-opening steps. In fact no direct dissociation of oxirane has been observed in our low-energy trajectories, and only occasionally does oxirane open its three-membered ring via C−C bond rupture to form CH_2OCH_2, which transforms back to oxirane shortly afterward. It is worth mentioning that as is the case with CH_2CH_2O, there are crossings of the triplet and singlet surfaces in the vicinity of the CH_2OCH_2 biradical. The short lifetime of the singlet CH_2OCH_2, however, precludes them from playing an important role in the ISC processes. The most frequent reaction of oxirane is to break the C−O bond back to CH_2CH_2O, which rearranges mainly to acetaldehyde. Similarly, vinyl alcohol most likely transforms to its more stable isomer acetaldehyde. Starting from acetaldehyde, there are several competing dissociation pathways: direct bond breakage to produce CH_3 + CHO, H + CH_3CO, and H + CH_2CHO (in the order of increasing dissociation energy) and molecular elimination to form CO + CH_4 and H_2 + CH_2CO. Although the CO and H_2 elimination pathways lead to products that are much lower in energy, the barriers to be surmounted are somewhat higher than the C−C bond dissociation energy, so that the C−C bond breaking to CH_3 + CHO is energetically slightly and dynamically more favorable. Due to the relatively long lifetime of these intermediate complexes, there are only three trajectories that successfully exit the deep valley of CH_3CHO in the first 4000 integration steps, and all lead to CH_3 + CHO.

After an initial propagation of 4000 steps (0.96 ps), the majority of reactive trajectories are still trapped as reaction intermediates (27 trajectories as $^3CH_2CH_2O$, 3 as $^1CH_2CH_2O$, 35 as acetaldehyde, 37 as oxirane, and 2 as vinyl alcohol). To determine their final dissociation pathways, we further propagated these trajectories for up to 20 400 steps (for a total of 5.76 ps). We find that the triplet CH_2CH_2O biradicals almost all decompose or transform to CH_3CHO, oxirane and CH_2CHOH within the first 14 000 integration steps. By 24 000 steps, all the triplet complexes have decayed. Thus the triplet to singlet ratio is converged to 25:75 in our direct dynamics TSH calculations, much lower than the experimental ratio of about 43:57.[5] To summarize, after 24 000 integration steps, there are a total of 41 trajectories dissociating on the triplet surface (14 as $OH + C_2H_3$, 21 as H + CH_2CHO, and 6 as $CH_2 + CH_2O$). At the same time, on the singlet surface, 69 trajectories are still trapped in the intermediate complex valleys (34 as acetaldehyde, 30 as oxirane, and 5 as vinyl alcohol). Of those singlets that do decay, 25 trajectories end up as CH_3 + CHO, 3 as H_2 + CH_2CO, 2 as CO + CH_4, 1 as H + CH_3CO, and 1 as H + CH_2CHO.

Figure 3 plots the reactive cross sections for formation of the various dissociation product pairs as a function of total integration time. This shows that dissociation on the triplet surface via the vinoxy and methylene channels occurs quickly relative to dissociation on the singlet surface. Dissociation of acetaldehyde gradually leads to the production of (mostly) CH_3 + CHO on the singlet surface, and eventually this will become the dominant product.

From these results, we can estimate the branching ratios for the primary product channels as follows. First, the $OH + C_2H_3$, H + CH_2CHO, and $CH_2 + CH_2O$ cross sections (2.8 ± 0.7 a_0^2, 5.3 ± 1.1 a_0^2, and 1.2 ± 0.5 a_0^2, respectively) on the triplet surface are converged because all triplet CH_2CH_2O have dissociated. On the singlet surface, ketene can be produced via the H_2 elimination from singlet CH_2CH_2O or from CH_3CHO. The three trajectories that give H_2 + CH_2CO all belong to the first category (the cross section is 1.4 ± 0.8 a_0^2). For the remaining singlet trajectories, we can assume that oxirane and CH_2CHOH will eventually convert to CH_3CHO, which further undergoes unimolecular decomposition to give product yields that can be determined by extrapolation. Compared to the C−C bond breakage product (CH_3 + CHO), the other dissociation channels (H + CH_3CO, H + CH_2CHO, CO + CH_4, and H_2 + CH_2CO) are minor. At the end of 0.96 ps, the CH_3 + CHO channel cross section is 0.7 ± 0.4 a_0^2, the other channels altogether are zero, which means a 100% rate of production for CH_3 + CHO. At 3.36 ps, the CH_3 cross section increases to 3.7 ± 0.9 a_0^2, but that of the other channels is only 0.1 ± 0.1 a_0^2 (97% branching for CH_3 + CHO). By 5.76 ps, the former becomes 6.3 ± 1.2 a_0^2, and the latter increases slightly to 0.2 ± 0.2 a_0^2 (96% for CH_3 + CHO). In a second set of 545 trajectories that we generated (described below) for a SOC of 50 cm^{-1}, the rate of production of CH_3 + CHO among the acetaldehyde reaction channels is found to be 70%. Nominally, this ratio should be the same no matter what the SOC is, as dissociation of acetaldehyde on the singlet surface is largely unaffected by the ISC processes. However, due to the high computational cost (~40 h per 4000 integration steps on a dual processor Opteron) in calculating B3LYP/6-31G(d,p) trajectories

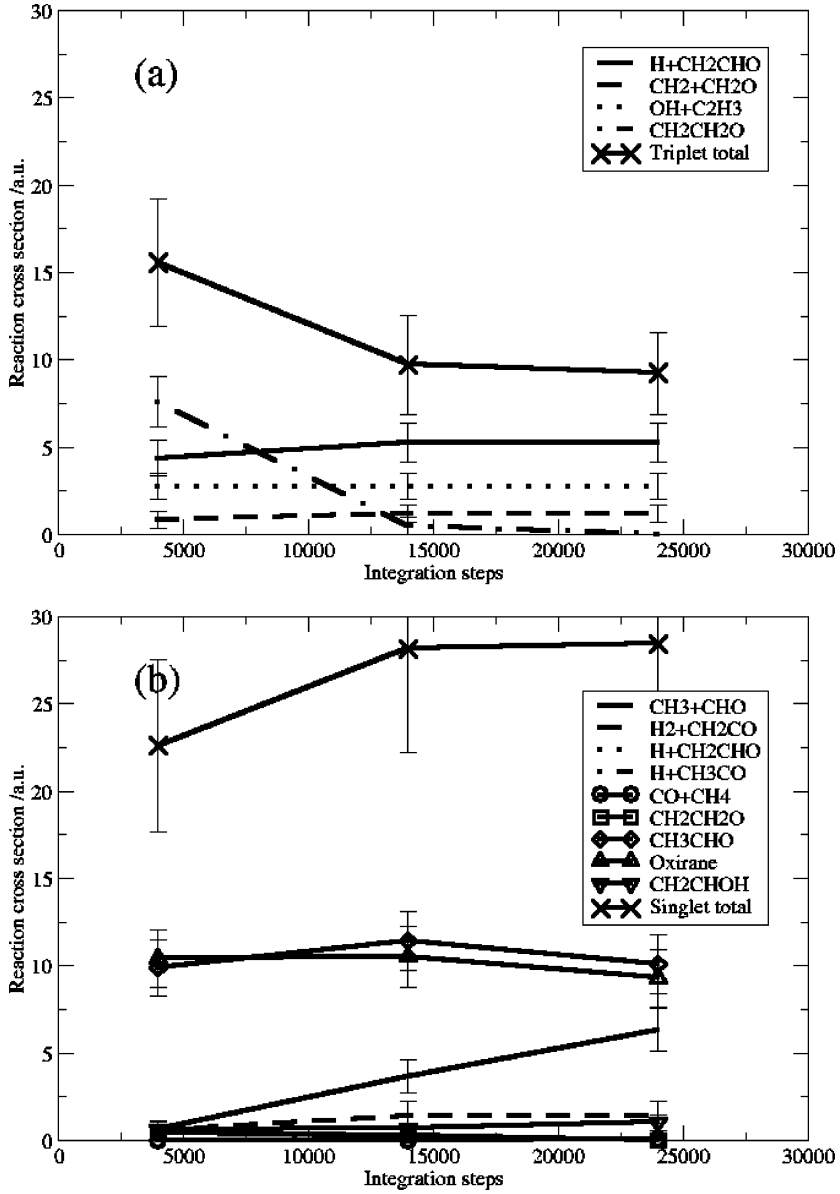

Figure 3. Reactive cross sections as a function of integration time for the observed dissociation products as well as for the major intermediate complexes on (a) the triplet surface and on (b) the singlet surface. The integration time step is 0.24 fs.

TABLE 1: Reactive Cross Sections (Units of a_0^2) of the Five Primary Product Channels from Our Direct Dynamics Calculations at Low and Hyperthermal Collision Energies

		H + CH_2CHO	CH_2 + CH_2O	OH + C_2H_3	CH_3 + CHO	H_2 + CH_2CO
E_{coll} = 0.56 eV	V_{13} = 70 cm^{-1}	5.3 ± 1.1	1.2 ± 0.5	2.8 ± 0.7	23.2 ± 4.4[a]	>1.4 ± 0.8 and <4.9 ± 1.5[a]
	V_{13} = 50 cm^{-1}	7.6 ± 1.8	1.0 ± 0.4	1.9 ± 0.6	18.5 ± 4.4[a]	>1.1 ± 0.6 and <4.4 ± 1.3[a]
E_{coll} = 3.0 eV	V_{13} = 70 cm^{-1}	8.3 ± 1.4	10.5 ± 1.6	7.4 ± 1.5	4.6 ± 1.1	0.3 ± 0.3

[a] These values are extrapolated from trajectories that remained trapped in local potential wells after an integration time of 5.76 ps as described in the text.

on the fly, the statistics of both sets of calculations is poor, corresponding to fewer than 30 trajectories dissociating on the singlet surface. To provide an overall estimate of the branching, we used an average value from the two sets of calculations, ~83%, for the branching fraction to give C−C bond breakage. This is a similar result to that obtained in the experiment, where the methyl channel is responsible for roughly 75% of all singlet products, assuming that channels R4 through R7 arise only from the singlet surface. Overall, the calculated cross section for the singlet intermediate complexes that have not dissociated by 5.76 ps is 20.4 ± 3.8 a_0^2, so, assuming that 83% of them decay via C−C breakage, the total CH_3 + CHO reactive cross section is estimated to be (6.3 + 20.4 × 83%) ± (1.2 + 3.8 × 83%) = 23.2 ± 4.4 a_0^2.

Table 1 tabulates the reactive cross sections (either calculated or estimated from our trajectory calculations) for the primary product channels at E_{coll} = 0.56 eV using a V_{13} = 70 cm^{-1}. The results obtained using a smaller V_{13} of 50 cm^{-1} as well as at a hyperthermal collision energy of 3.0 eV are also listed. We further compare in Table 2 our calculated branching ratios for these products with those from the experiment at E_{coll} = 0.56 eV. Obviously the two product channels that are much overestimated are OH + C_2H_3 and CH_3 + CHO. The former is due to an H abstraction barrier on the B3LYP surface that is

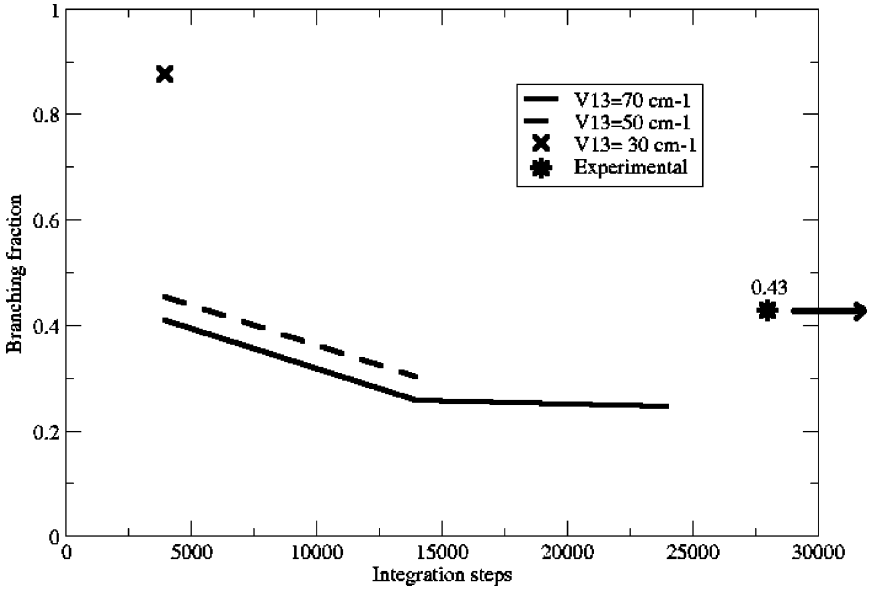

Figure 4. Branching fractions $\sigma_i/\Sigma_i\sigma_i$ for the triplet products when different values of the spin−orbit coupling V_{13} are used to compute the transition probabilities at the triplet−singlet crossing points. The experimental value[5] is 0.43. The integration time step is 0.24 fs.

TABLE 2: Product Relative Yields for the O(^{3}P) + C_2H_4 Reaction at E_{coll} = 0.56 eV

		H + CH_2CHO	CH_2 + CH_2O	OH + C_2H_3	CH_3 + CHO	H_2 + CH_2CO
theory	V_{13} = 70 cm^{-1}	14 ± 6%	3 ± 2%	7 ± 4%	62 ± 27%	>1% and <20%
	V_{13} = 50 cm^{-1}	22 ± 12%	3 ± 2%	6 ± 3%	55 ± 29%	>0% and <21%
experiment[5]		27 ± 6%	16 ± 8%		43 ± 11%	13 ± 3%

too low. In fact, this channel has not been observed in low-energy experiments. The 62% relative yield of the methyl channel (the experimental branching is 43%) can only be explained by too much ISC in our trajectory calculations. We assess this point later when we present results for smaller SOC values.

There has been much uncertainty in past experimental work concerning the yield of the ketene channel, the second most important dissociation product on the singlet surface. As discussed above, H_2 + CH_2CO comes from either direct dissociation of singlet CH_2CH_2O or unimolecular decomposition of acetaldehyde. Our trajectories show that the first route dominates for short propagation times, and by 5.76 ps the ketene formation cross section is 1.4 ± 0.8 a_0^2 (corresponding to 4% of the total yield), comparable to the methylene channel cross section of 1.2 ± 0.5 a_0^2. Given longer integration times, the ketene channel will increase due to H_2 elimination from acetaldehyde. This gives us a lower bound of 1% for the ketene channel. An upper bound can be determined by assuming that all of the acetaldehyde, which does not dissociate to give the methyl channel gives the ketene channel instead. This gives an estimate of <20% as noted in Table 2. As to the triplet products H + CH_2CHO and CH_2 + CH_2O, their yields are underestimated due to the overestimated ISC. In particular, the branching ratio of the methylene channel is only ~22% of that of the vinoxy channel, lower than the experimental value of about 60%. [Our RRKM calculations revealed a ratio of about 54%, which is closer to the experiment. This defect in our trajectory calculations concerning the underestimated methylene to vinoxy channel ratio is most likely due to the limited number of DFT trajectories we could run on systems like O + C_2H_4.]

We tested two smaller values of SOC, 50 and 30 cm^{-1}, for calculating the transition probabilities at the T−S crossing points along the trajectories. The ratios of the triplet to singlet yields are compared in Figure 4 for the three values of the SOC parameter used in the direct dynamics simulations. It is found that a V_{13} of 50 cm^{-1} still results in too much ISC in the trajectory output, with the triplet to singlet ratio being 30:70 and the experimental ratio being 43:57. When V_{13} is further decreased to 30 cm^{-1}, there is a noticeable reduction in intersystem crossing, such that after 4000 steps the triplet to singlet branching is 88:12. Propagating the trajectories for longer times will result in more intersystem crossing but is not expected to bring down this ratio to close to the experimental value.[40] Thus to match experimental triplet/singlet branching, a SOC between 30 and 50 cm^{-1} is needed. This would be comparable to that estimated from our CASSCF calculations (35 cm^{-1}) as described earlier. However, a precise match with experiment using the CASSCF value is not expected due to approximations in the dynamics calculations. There are a variety of factors in the TSH method that would lead to deviations between theory and experiment, including the quality of the potential energy surfaces, the neglect of surface hopping away from the intersection points, and approximations in the basic TSH algorithm. Past comparisons of more sophisticated TSH calculations with accurate quantum results[17,41,42] suggest that transition probabilities can often be off by a factor of 2, so in this respect, the agreement between theory and experiment in the present application is actually quite good.

On the basis of calculations using V_{13} = 50 cm^{-1}, we determined the product branching ratios that are also listed in Table 2. It is shown that the methyl channel relative yield decreases to 55% and the vinoxy channel increases to 22% due to a reduction in ISC when SOC is lowered from 70 to 50 cm^{-1}. However, we do not see a corresponding increase in the methylene channel relative yield. Both the methylene and the ketene channels are underestimated as compared to the experiment.

We now examine the product angular distributions for the vinoxy channel, the methyl channel, and the hydroxyl channel, obtained at 5.76 ps integration time with the SOC parameter of 70 cm^{-1}. The OH center-of-mass angular distribution shows a

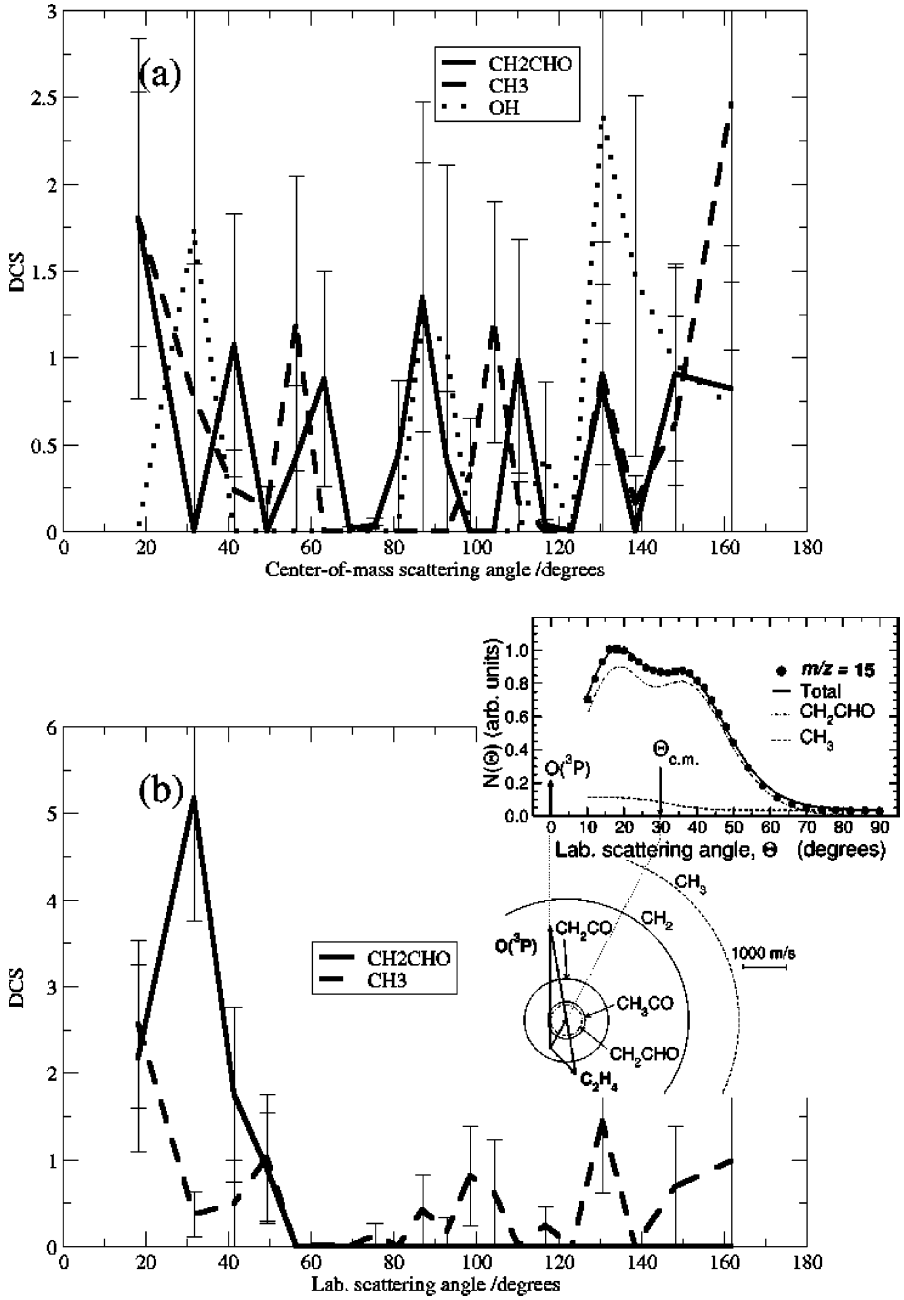

Figure 5. Angular distributions expressed as normalized differential cross sections (DCS, $(2\pi/\sigma)(d\sigma/d\Omega')$) in (a) the center-of-mass frame and (b) the laboratory frame for the vinoxy and methyl products from the B3LYP trajectory calculations. The inset shows the lab distribution and the Newton circle from the experiment.[5]

small preference for the backward direction with respect to the incoming oxygen atom (Figure 5a), which is consistent with a rebound mechanism for direct abstraction in which O attacks along the C−H bond and the resulting OH bounces back the same way. The angular distributions for CH_2CHO and CH_3 are almost forward−backward symmetric, which is typical of reactions that proceed through long-lived intermediate complexes. The Casavecchia et al. experiment measured the lab frame angular distributions for CH_2CHO and CH_3. By converting the velocities into the lab frame, we obtain lab angular distributions that can be compared with the experiment (Figure 5b). We see qualitative agreement between theory and experiment, with CH_2CHO scattered in the forward hemisphere and CH_3 scattered in all directions, consistent with the picture that can be drawn from the Newton diagram.

3C. Dynamics at Hyperthermal Energy. Collisions of the reactant molecules in the hyperthermal regime allow areas of the PES that are forbidden at low energy to be accessed; therefore, high-energy barrier reaction pathways are now open, as well as secondary steps in which the products further dissociate. In addition, as the reactivity on the triplet surface is very much enhanced, ISC plays a less important role at high energies.

A total of 592 trajectories were calculated for $E_{coll} = 3.0$ eV (69.2 kcal/mol), among which 236 are reactive. We integrated the trajectories for a maximum of 4000 steps (0.96 ps), and only 20 trajectories are trapped as intermediate complexes at the end of the propagation (1 as triplet CH_2CH_2O, 5 as oxirane, 3 as acetaldehyde, 2 as triplet CH_2CHOH, and 9 as singlet CH_2-CHOH). The triplet yield versus the singlet yield is determined to be 71:29, much larger than for low-energy trajectories (25:75). Note that we still use a SOC of 70 cm^{-1} in these calculations, so the formation of singlet products is likely less important than we estimate.

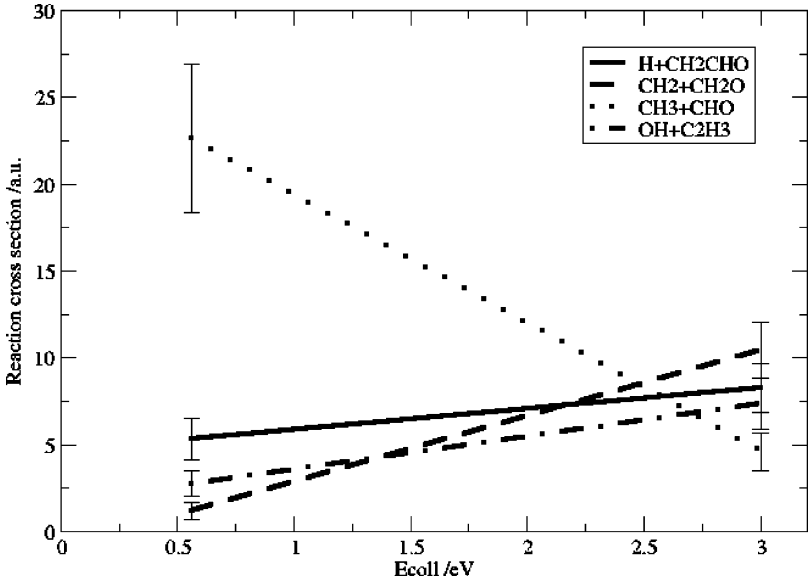

Figure 6. Reactive cross sections for the primary dissociation products at 0.56 and 3.0 eV collision energies.

Another noticeable difference is an increase in importance of the CH_2CHOH channel at high energies. As we discussed earlier, vinyl alcohol is the least favorable among the CH_2CH_2O isomerization reactions on the singlet surface. As the collision energy increases, however, isomerization of the triplet CH_2CH_2O biradical is possible in addition to the direct decomposition to $H + CH_2CHO$ and $CH_2 + CH_2O$. We even observed one trajectory that undergoes a $^3CH_2CH_2O \xrightarrow{TS9} {}^3CH_2O{-}CH_2$ transformation on the triplet surface, for which the barrier is as high as 57.2 kcal/mol. So a considerable amount of CH_2CHOH can be produced in the triplet state. The triplet and singlet surfaces cross close to the triplet configuration of CH_2CHOH, so when a trajectory is trapped in the triplet CH_2CHOH valley, surface hops to the singlet state are possible. This provides an alternative route to the formation of CH_2CHOH in the singlet state. Starting from triplet and singlet CH_2CHOH, a variety of decomposition channels are now accessible: O−H bond breakage to give $H + CH_2CHO$, C−O bond breaking to $OH + C_2H_3$, C−H bond breaking to $H + CH_2COH$ or $H + CHCH(OH)$, and even molecular elimination to $H_2O + C_2H_2$ or $H_2O + CH_2C$. The $^3CH_2CH_2O \rightarrow {}^3CH_3CHO$ isomerization is another important reaction on the triplet surface, which subsequently leads to mainly $CH_3 + CHO$ via C−C bond breakage.

The above mechanisms are still minor channels compared to CH_2CH_2O dissociation to $H + CH_2CHO$ and $CH_2 + CH_2O$ on the triplet surface and to acetaldehyde C−C breakage to give $CH_3 + CHO$ on the singlet surface. There is also an increase in the production of $CO + CH_4$ from acetaldehyde. We should emphasize that products that exclusively come from the singlet surface such as $CH_3 + CHO$ and $H_2 + CH_2CO$, or exclusively come from the triplet surface such as $OH + C_2H_3$, $H + CH_2CHO$, and $CH_2 + CH_2O$ in low-energy collisions, can now be produced by both triplet and singlet mechanisms. For instance, about 37% of the total $CH_3 + CHO$ yield arises from triplet CH_3CHO decomposition. In Figure 6, we plot the reactive cross sections as function of collision energy for the four major dissociation products. Due to diminished ISC, the $OH + C_2H_3$, $H + CH_2CHO$, and $CH_2 + CH_2O$ channels, which originate mainly from reactions on the triplet surface, dominate the overall product yields at 3.0 eV collision energy. The $CH_3 + CHO$ channel, which is the primary product at 0.56 eV, gradually loses its dominance to other channels as the collision energy increases. The methylene cross section increases much more rapidly with increasing energy than do vinoxy and hydroxyl channels so that $CH_2 + CH_2O$ becomes the most abundant product at 3.0 eV. In summary, our computed product branching ratios at 3.0 eV are as follows: $32 \pm 14\%$ for $CH_2 + CH_2O$, $25 \pm 12\%$ for $H + CH_2CHO$, $23 \pm 11\%$ for $OH + C_2H_3$, $14 \pm 8\%$ for $CH_3 + CHO$, $4 \pm 3\%$ for $CO + (CH_4$ or $CH_3 + H$, or $CH_2 + H_2)$, and roughly 1% for $H_2 + CH_2CO$.

4. Conclusions

We studied intersystem crossing effects in the $O(^3P) + C_2H_4$ reaction dynamics for two regimes of collision energy; one at 0.56 eV to simulate a low-energy crossed molecular beam experiment, and the other at 3.0 eV to study nonadiabatic dynamics at hyperthermal energy. We used a simplified version of the quasiclassical trajectory surface hopping method in which triplet−singlet transitions are only allowed at points where the two surfaces cross. The Landau−Zener model was employed to calculate the transition probabilities with a constant SOC at all crossing points. The potential energy surfaces are calculated as the trajectories evolve by using the unrestricted B3LYP/6-31G(d, p) electronic structure method. ISC effects were shown to be sensitive to the value of the SOC parameter used in calculating the hopping probabilities, with V_{13} of 70 or 50 cm^{-1} overestimating the rate of triplet → singlet transitions and 30 cm^{-1} underestimating it at 0.56 eV. The optimum value of about 40 cm^{-1} estimated from this analysis is comparable to estimates using CASSCF calculations of the average SOC matrix elements, which indicates that errors in the TSH dynamics approach and in the PES are not serious.

In our calculations based on a SOC of 70 cm^{-1}, the singlet product $CH_3 + CHO$ accounts for $62 \pm 27\%$ of the overall reaction yield (the experimental ratio is $43 \pm 11\%$), followed by the triplet product $H + CH_2CHO$ ($14 \pm 6\%$ versus the experimental $27 \pm 6\%$). The 50 cm^{-1} SOC brings down the singlet ratio and leads to better agreement with experiment for the relative yields of the methyl and vinoxy channels. The calculations also show overestimation of the hydroxyl channel and underestimation of the methylene channel due largely to defects in the B3LYP surface. As we go to higher collision energy (3 eV), ISC plays a much less important role due to the enhanced reactivity on the triplet surface, and shortened lifetimes of the intermediate complex, and as a result triplet products dominate over singlet products. The importance of the methylene

+ formaldehyde channel exceeds that of the H + vinoxy and methyl + CHO channels, and methylene + CH_2O becomes the most abundant product. Some novel reaction channels that are inaccessible at low energy are also found.

Acknowledgment. This research was supported by AFOSR Grant FA9550-07-1-0095 and by the Hungarian National Scientific Research Fund grant T49257.

References and Notes

(1) Gardiner, W. C., Jr. *Gas-Phase Combustion Chemistry*; Springer-Verlag: New York, 2000.
(2) Cvetanović, R. J. *J. Chem. Phys*. **1955**, *23*, 1375.
(3) Cvetanović, R. J. *Adv. Photochem*. **1963**, *1*, 115.
(4) Cvetanović, R. J. *J. Phys. Chem*. **1970**, *74*, 2730.
(5) Casavecchia, P.; Capozza, G.; Segoloni, E.; Leonori, F.; Balucani, N.; Volpi, G. G. *J. Phys. Chem. A* **2005**, *109*, 3527 and the references therein.
(6) Bader, R. F. W.; Stephens, M. E.; Gangi, R. A. *Can. J. Chem*. **1977**, *55*, 2755.
(7) Dupuis, M.; Wendoloski, J. J.; Takada, T.; Lester, W. A., Jr. *J. Chem. Phys*. **1982**, *76*, 481.
(8) Wortmann-Saleh, D.; Engels, B.; Peyerimhoff, S. D. *J. Phys. Chem*. **1994**, *98*, 9541.
(9) Baulch, D. L.; Cobos, C. J.; Cox, R. A.; Frank, P.; Hayman, G.; Just, Th.; Kerr, J. A.; Murrells, T.; Pilling, M. J.; Troe, J.; Walker, R. W.; Warnatz, J. *J. Phys. Chem. Ref. Data* **1994**, *23*, 847.
(10) Yamaguchi, K.; Yabushita, S.; Fueno, T., Kato, S.; Morokuma, K. *Chem. Phys. Lett*. **1980**, *70*, 27.
(11) Fueno, T.; Takahara, Y.; Yamaguchi, K. *Chem. Phys. Lett*. **1990**, *167*, 291.
(12) Melius, C. F. unpublished results cited in Schmoltner, A. M.; Chu, P. M.; Brudzynski, R. J.; Lee, Y. T. *J. Chem. Phys*. **1989**, *91*, 6926.
(13) Jursic, B. S. *THEOCHEM* **1999**, *492*, 85.
(14) Smith, B. J.; Nguyen, M. T.; Bouma, W. J.; Radom, L. *J. Am. Chem. Soc*. **1991**, *113*, 6452.
(15) Joshi, A.; You, X.; Barckholtz, T. A.; Wang, H. *J. Phys. Chem. A* **2005**, *109*, 8016.
(16) Nguyen, T. L.; Vereecken, L.; Hou, X. J.; Nguyen, M. T.; Peeters, J. *J. Phys. Chem. A* **2005**, *109*, 7489.
(17) Hoffmann, M. R.; Schatz, G. C. *J. Chem. Phys*. **2000**, *113*, 9456.
(18) Maiti, B.; Schatz, G. C. *J. Chem. Phys*. **2003**, *119*, 12360.
(19) Maiti, B.; Schatz, G. C.; Lendvay, G. *J. Phys. Chem. A* **2004**, *108*, 8772.
(20) Stine, J. R.; Muckerman, J. T. *J. Chem. Phys*. **1976**, *65*, 3975; **1978**, *68*, 185.
(21) Tully, J. C. *J. Chem. Phys*. **1990**, *93*, 1061.
(22) Meyer, H. -D.; Miller, W. H. *J. Chem. Phys*. **1979**, *70*, 3214.
(23) Gerber, R. B.; Buch, V.; Ratner, M. A. *J. Chem. Phys*. **1982**, *77*, 3022.
(24) Buch, V.; Gerber, R. B.; Ratner, M. A. *Chem. Phys. Lett*. **1983**, *101*, 44.
(25) Micha, D. A. *J. Chem. Phys*. **1983**, *78*, 7138.
(26) Durup, J. *Chem. Phys. Lett*. **1990**, *173*, 537.
(27) Alimi, R.; Gerber, R. B.; Hammerich, A. D.; Kosloff, R.; Ratner, M. A. *J. Chem. Phys*. **1990**, *93*, 6484.
(28) García-Vela, A.; Gerber, R. B.; Imre, D. G. *J. Chem. Phys*. **1992**, *97*, 7242.
(29) Kong, J.; White, C. A.; Krylov, A. I.; Sherrill, C. D.; Adamson, R. D.; Furlani, T. R.; Lee, M. S.; Lee, A. M.; Gwaltney, S. R.; Adams, T. R.; Ochsenfeld, C.; Gilbert, A. T. B.; Kedziora, G. S.; Rassolov, V. A.; Maurice, D. R.; Nair, N.; Shao, Y.; Besley, N. A.; Maslen, P. E.; Dombroski, J. P.; Dachsel, H.; Zhang, W. M.; Korambath, P. P.; Baker, J.; Byrd, E. F. C.; Van Voorhis, T.; Oumi, M.; Hirata, S.; Hsu, C. P.; Ishikawa, N.; Florian, J.; Warshel, A.; Johnson, B. G.; Gill, P. M. W.; Head-Gordon, M.; Pople, J. A. *Q-Chem*, Version 2.0; Q-Chem, Inc.: Export, PA, 2000.
(30) Becke, A. D. *J. Chem. Phys*. **1993**, *98*, 5648.
(31) Lee, C.; Yang, W.; Parr, R. G. *Phys. Rev. B* **1988**, *37*, 785.
(32) Knuts, S.; Minaev, B.; Vahtras, O.; Ågren, H. *Int. J. Quantum Chem*. **1995**, *55*, 23.
(33) Fedorov, D. G.; Gordon, M. S. *J. Chem. Phys*. **2000**, *112*, 5611.
(34) Schmidt, M. W.; Baldridge, K. K.; Boatz, J. A.; Elbert, S. T.; Gordon, M. S.; Jensen, J. H.; Koseki, S.; Matsunaga, N.; Nguyen, K. A.; Su, S. J.; Windus, T. L.; Dupuis, M.; Montgomery, J. A. *J. Comput. Chem*. **1993**, *14*, 1347.
(35) Dunning, T. H., Jr. *J. Chem. Phys*. **1989**, *90*, 1007.
(36) Zhu, C.; Nakamura, H. *J. Chem. Phys*. **1995**, *102*, 7448; **1997**, *106*, 2599.
(37) Zhu, C.; Teranishi, Y.; Nakamura, H. *Adv. Chem. Phys*. **2001**, *117*, 127.
(38) Camden, J. P.; Bechtel, H. A.; Brown, D. J. A.; Martin, M. R.; Zare, R. N.; Hu, W.; Lendvay, G.; Troya, D.; Schatz, G. C. *J. Am. Chem. Soc*. **2005**, *127*, 11898.
(39) Camden, J. P.; Hu, W.; Bechtel, H. A.; Brown, D. J. A.; Martin, M. R.; Zare, R. N.; Lendvay, G.; Troya, D.; Schatz, G. C. *J. Phys. Chem. A* **2006**, *110*, 677. Hu, W.; Lendvay, G.; Troya, D.; Schatz, G. C.; Camden, J. P.; Bechtel, H. A.; Brown, D. J. A.; Martin, M. R.; Zare, R. N. *J. Phys. Chem. A* **2006**, *110*, 3017.
(40) We observed that, for a SOC = 30 cm^{-1}, at the end of 4000 integration steps, the ratio between the triplet trajectories that had already dissociated (the cross section was ~8.5 a_0^2) and all the singlet trajectories (the cross section was ~4.1 a_0^2) was 2:1, which means that in the triplet CH_2CH_2O biradical region, ISC cannot compete with direct dissociation on the triplet surface. To estimate a lower bound to the final triplet to singlet ratio, we assume a 1:1 ratio between direct dissociation on the triplet surface and ISC to the singlet surface for the triplet biradicals that remain after 4000 steps (the cross section was ~20.5 a_0^2). This yields a triplet to singlet ratio $>(8.5 + 20.5 \times 0.5)/(4.1 + 20.5 \times 0.5) \approx 57:43$.
(41) Gray, S. K.; Petrongolo, C.; Drukker, K.; Schatz, G. C. *J. Phys. Chem. A* **1999**, *103*, 9448.
(42) Gray, S. K.; Balint-Kurti, G. G.; Schatz, G. C.; Lin, J. J.; Liu, X.; Harich, S.; Yang, X. *J. Chem. Phys*. **2000**, *113*, 7330.